

## TGF $\beta$ Signaling Promotes Juvenile Granulosa Cell Tumorigenesis by Suppressing Apoptosis

Nadéra Mansouri-Attia,\* Swamy K. Tripurani,\* Nisha Gokul, Hermann Piard, Matthew L. Anderson, Karen Eldin, and Stephanie A. Pangas

Department of Pathology and Immunology (N.M.-A., S.K.T., H.P., M.L.A., K.E., S.A.P.), Department of Obstetrics and Gynecology (M.L.A.), Graduate Program in Molecular and Cell Biology (N.G.), and Department of Molecular and Cellular Biology (S.A.P.), Baylor College of Medicine, Houston, Texas 77030

Molecular changes that give rise to granulosa cell tumors of the ovary are not well understood. Previously, we showed that deletion in granulosa cells of the bone morphogenetic protein receptor-signaling transcription factors, *Smad1* and *Smad5*, causes development of metastatic granulosa cell tumors that phenocopy the juvenile form of granulosa cell tumors (JGCTs) in humans. The TGF $\beta$ -SMAD2/3 pathway is active in JGCTs, but its role is unknown. We tested the *in vivo* contribution of TGF $\beta$ -SMAD signaling to JGCT development by genetically deleting the common *Smad4* from *Smad1/5* double knockout mice. *Smad1/5/4* triple knockout mice were sterile and had significantly increased survival and delayed tumor development compared to those for the *Smad1/5* double knockout mice. The few tumors that did develop were smaller, showed no evidence of metastasis, and had increased apoptosis. In the human JGCT cell line COV434, TGF $\beta$ 1 increased viability by inhibiting apoptosis through a TGF $\beta$  type I receptor-dependent repression of caspase activity and inhibition of poly(ADP-ribose) polymerase cleavage. These data support a tumor-promoting function of TGF $\beta$  in JGCTs through its ability to repress apoptosis. (*Molecular Endocrinology* 28: 1887–1898, 2014)

**G**ranulosa cell tumors (GCTs) are a form of sex cord stromal neoplasms representing approximately 5% of all ovarian tumors (1). There are 2 histologic forms: a pediatric/juvenile type (JGCT), an aggressive form that usually occurs in patients younger than 20 years of age, and the adult type (AGCT), which is more common. These 2 forms of GCTs are classified on clinical and pathologic criteria, such as tumor histology, nuclear morphology, and the potential for disease recurrence and may represent different diseases with dissimilar etiologies (2, 3). In contrast to their occurrence in humans, GCTs have a high incidence in some breeds of dogs and domestic animals, as well as small mammals, such as mice (4, 5). A somatic mutation in the forkhead box L2 (*FOXL2*) gene

is pathognomonic of almost all AGCTs, but most JGCTs lack this mutation and are not known to contain a consistent mutation profile (3, 6).

Previously, we showed that double conditional deletion of the bone morphogenetic protein (BMP) receptor signaling SMAD transcription factors in mouse ovaries (*Smad1/5* double conditional knockout [dKO] mice) results in GCTs with full penetrance (7). Microscopic tumors are histologically visible in the ovary by 8 weeks of age and develop into large ovarian tumors with peritoneal metastases that increase with age (7). The disease profile in *Smad1/5* dKO mice is similar to that of human JGCTs (8). Mice null for the inhibin  $\alpha$ -subunit (*Inha*<sup>-/-</sup>) also develop GCTs of mixed granulosa/Sertoli cells with a

ISSN Print 0888-8809 ISSN Online 1944-9917

Printed in U.S.A.

Copyright © 2014 by the Endocrine Society

Received July 17, 2014. Accepted September 16, 2014.

First Published Online September 22, 2014

\* N.M.-A. and S.K.T. contributed equally to the study.

Abbreviations: AGCT, adult granulosa cell tumor; BMP, bone morphogenetic protein; cKO, conditional knockout; DAPI, 4',6-diamidino-2-phenylindole; dKO, double conditional knockout; FITC, fluorescein isothiocyanate; GCT, granulosa cell tumor; HSD, honestly significant difference; JGCT, juvenile granulosa cell tumor; MTS, 3-(4,5-dimethylthiazol-2-yl)-5-(3-carboxymethoxyphenyl)-2-(4-sulfophenyl)-2H-tetrazolium, inner salt; qPCR, quantitative real-time PCR; PARP, poly(ADP-ribose) polymerase; rh, recombinant human; tKO, triple conditional knockout; TUNEL, terminal deoxynucleotidyl transferase dUTP nick-end labeling.

slightly different histologic pattern, and this is further accompanied by a severe cachexia-like wasting syndrome driven primarily by activin signaling (9, 10). The canonical signaling pathway for activin, as well as TGF $\beta$ , is through the intracellular transcription factors, SMAD2 and SMAD3, and deletion of *Smad3* from *Inha*<sup>-/-</sup> mice slows tumor development (11–13). Once phosphorylated by the activated TGF $\beta$  type I receptors, SMAD2 and SMAD3 form trimeric complexes with the common SMAD4 and accumulate in the nucleus to regulate gene transcription (14). GCTs and metastatic tumors from *Smad1/5* dKO mice and *Inha*<sup>-/-</sup> mice, as well as human JGCT samples, display an active SMAD2/3 pathway as demonstrated by a strong immunoreactivity for nuclear phospho-SMAD2/3 (7, 8). These data suggest that SMAD2/3 activation could play a crucial role in granulosa cell tumorigenesis. However, it is unclear whether SMAD2/3 activation stems from changes in TGF $\beta$  signaling, activin signaling, or both. Therefore, the objective of this study was to determine the contribution of activin and TGF $\beta$ -driven SMAD signaling during development of JGCT in *Smad1/5* dKO mice and humans.

## Materials and Methods

### Generation of *Smad4*, *Smad1/5*, and *Smad1/5/4* conditional knockout (cKO) mice

Experimental animals were maintained on a C57BL/6J/129S7/SvEvBrd mixed hybrid background and used in accordance with the National Institutes of Health Guide for the Care and Use of Laboratory Animals and approved animal protocols at Baylor College of Medicine. *Smad1*, *Smad5*, and *Amhr2*<sup>cre</sup> conditional alleles and generation of *Smad1/5* dKO mice were described in detail previously (7). *Smad1*<sup>flox/flox</sup>*Smad5*<sup>flox/flox</sup>*Amhr2*<sup>cre+</sup> mice are referred to as *Smad1/5* dKO mice. Generation of the *Smad4* conditional allele and *Smad4*<sup>flox/-</sup>*Amhr2*<sup>cre+/+</sup> cKO mice was described elsewhere (15). Experimental mice (*Smad1*<sup>flox/flox</sup>*Smad5*<sup>flox/flox</sup>*Smad4*<sup>flox/flox</sup>*Amhr2*<sup>cre+/+</sup>) (referred to here as *Smad1/5/4* triple conditional knockout [tKO]) were generated by crossing *Smad1*<sup>flox/flox</sup>*Smad5*<sup>flox/flox</sup>*Smad4*<sup>flox/flox</sup>*Amhr2*<sup>cre+</sup> males with *Smad1*<sup>flox/flox</sup>*Smad5*<sup>flox/flox</sup>*Smad4*<sup>flox/flox</sup> females. Littermates that were wild type at the *Amhr2* locus served as controls.

### Fertility analysis

To assess the reproductive performance of *Smad1/5/4* tKO female mice, six individually housed 6-week-old control females (*Smad1*<sup>flox/flox</sup>*Smad5*<sup>flox/flox</sup>*Smad4*<sup>flox/flox</sup>) or *Smad1/5/4* tKO littermates were bred to wild-type F1 hybrid males with known fertility. The number of litters and pups born per litter were recorded over a 6-month period. Fertility analyses of *Smad4* cKO and *Smad1/5* dKO were described previously (7, 15).

### Tissue collection

Mice were anesthetized by isoflurane inhalation (Butler Schein) and killed by cervical dislocation. Tissues were fixed in

10% neutral-buffered formalin (Fisher Scientific) overnight or stored in RNAlater (Ambion) at -80°C. Granulosa cells were collected as described previously (16).

### Patient study approval

Archived, deidentified, formalin-fixed, paraffin-embedded JGCT samples from surgical resections were acquired from the Department of Pathology's Tissue Bank at Texas Children's Hospital (Houston, Texas) as described previously (8). Deidentified patient data are shown in Supplemental Table 1. Tissues were treated in accordance with Baylor College of Medicine Institutional Review Board approval and a waiver of consent was approved (Institutional Review Board H-23139). Four samples of JGCTs from patients ranging in age from 10 months to 15 years were examined. Pathological assessment was performed by the Department of Pathology at Texas Children's Hospital. Specimens of normal premenopausal ovaries were obtained from the Gynecologic Tissue Biorepository at Baylor College of Medicine (Institutional Review Board H-26633). Written informed consent was obtained from all study subjects. Only specimens collected from women undergoing surgery for benign indications were used. No specimens were collected from women undergoing surgery for endometriosis.

### Histological analysis and immunohistochemistry

Mouse tissue was processed and embedded in paraffin by the Department of Pathology Tissue Acquisition and Pathology Core (Baylor College of Medicine) using standard protocols. Immunohistochemical analysis was performed using a Vectastain ABC kit (Vector Laboratories) according to the manufacturer's instructions in triplicate on a minimum of 3 samples, with negative controls (primary antibody omitted) run in parallel. Tissue sections were incubated overnight at 4°C with rabbit anti-inhibin  $\alpha$  (1:500; a gift of W. Vale, Salk Institute, La Jolla, California). Immunoreactivity was visualized by 3,3'-diaminobenzidine horseradish substrate (Vector Laboratories), and tissue was counterstained with hematoxylin.

### Atretic follicle counts

Atretic follicle counts were performed similarly to a previously described method (15, 17, 18). In brief, ovaries were fixed overnight in 10% neutral buffered formalin and embedded following standard protocols. Sections (7- $\mu$ m-thick) were stained with the periodic acid-Schiff reaction and hematoxylin. At least 3 ovaries were analyzed for each genotype. Follicles were counted from 5 of the largest cross sections and normalized to the total area of the section. Any follicle with discontinuous basement membrane, collapsed zona pellucida, pyknotic nuclei in granulosa cells, shrunken irregularly shaped oocytes, and irregular follicle size was considered to be an atretic follicle. Measurements and the area of the ovary were collected using AxioVision 4.0 software (Carl Zeiss) and plotted as the average number of atretic follicles per millimeter squared compared with their respective controls.

### COV434 cell culture and reagents

An immortalized human JGCT cell line (COV434) was purchased from Public Health England culture collections and maintained as described previously (19). For TGF $\beta$  experiments, cells were treated for 30 minutes with DMSO (0.1%) as

a control, with TGF $\beta$ 1 (2.5 ng/mL), or with a 30-minute preincubation with SB-505124 (10  $\mu$ M), a selective inhibitor of the TGF $\beta$  family type I receptors (ALK4, ALK5, and ALK7) (20) before TGF $\beta$ 1 addition. SB-505124 was developed as a competitive inhibitor of the ATP-binding pocket of ALK5, and concentrations of 10  $\mu$ M SB-505124 have few off-target effects (20, 21). SB-505124 has been used to inhibit the TGF $\beta$ 1 and TGF $\beta$ 2 isoforms in a number of cell lines, including cancer cell lines (22–26). For activin experiments, cells were treated for 30 minutes with PBS (0.1%) (control), with activin A (25 ng/mL) alone, or with a 30-minute preincubation with follistatin (400 ng/mL).

### RNA extraction and RT-PCR

Total RNA was extracted using an RNeasy Micro Kit according to the manufacturer's instructions (QIAGEN). cDNA synthesis from total RNA was performed using High Capacity RNA-to-cDNA Master Mix (Life Technologies) according to the manufacturer's instructions. The mRNA expression profile of selected genes was analyzed by quantitative real-time PCR (qPCR) using a StepOnePlus Real-Time PCR System and Fast SYBR Green Master Mix (Life Technologies). Melt curve analysis was used to verify a single amplification peak. Data were analyzed using the  $\Delta\Delta C_T$  method, normalized to the endogenous reference (*Gapdh*) and are expressed relative to the control samples, similar to previous studies (19). Primers used for mice and human samples are listed in Supplemental Tables 2 and 3.

### Protein extraction and immunoblot analysis

After treatment, cells were washed with cold PBS and resuspended in lysis buffer (T-PER tissue protein extraction reagent; Thermo Scientific) containing phosphatase and protease inhibitors (Roche). Cell lysates were incubated on ice for 30 minutes and then were centrifuged at 13 000 rpm for 10 minutes at 4°C. The supernatants were electrophoresed through a 4% to 12% bis-Tris gel (Life Technology), transferred to a polyvinylidene difluoride membrane, and blocked in 1× Tris-buffered saline with 0.1% Tween-20 (TBS-T) supplemented with 5% of nonfat milk for 2 hours, followed by incubation overnight at 4°C with primary antibodies (1:1000 dilution; Cell Signaling Technology): rabbit anti-phospho-SMAD2/3 Ser465/467, rabbit anti-SMAD2, rabbit anti-poly(ADP-ribose) polymerase (PARP) 1, rabbit anti-cleaved-PARP1, or a horseradish peroxidase-conjugated mouse anti- $\beta$  actin antibody (Santa Cruz Biotechnology) (1:10 000). After several washes, blots were incubated with peroxidase-labeled secondary antibody (Jackson ImmunoResearch) diluted at 1:5000 or 1:2000 (for PARP1 and cleaved-PARP1 immunoblots) in blocking solution for 1 hour. The membranes were washed with TBS-T and detected with Super-Signal West Pico Chemiluminescent Substrate (Pierce). Immunoblots were quantified using the Alpha Innotech FluorChem Q (Protein Simple).

### 3-(4,5-Dimethylthiazol-2-yl)-5-(3-carboxymethoxyphenyl)-2-(4-sulfophenyl)-2H-tetrazolium, inner salt (MTS) assay

COV434 cells were cultured in a 24-well plate at a density of  $5 \times 10^4$  cells/well and treated as indicated. After 3 days, Cell Titer 96 AQueous nonradioactive cell proliferation assay solution (Promega) was added to each well according to the manufacturer's instructions. After 3 hours of incubation at 37°C and

5% CO<sub>2</sub>, cell viability was determined by measuring the absorbance at 490 nm using a 550 plate reader (Bio-Rad Laboratories).

### Fluorescein isothiocyanate (FITC) annexin V apoptotic assay (flow cytometry)

COV434 cells were plated at a density of  $10^5$  cells/well in a 24-well plate and then were treated with DMSO (0.1%) as a control, TGF $\beta$ 1 (2.5 ng/mL) alone, SB-505124 (10  $\mu$ M), or a combination of both TGF $\beta$ 1 (2.5 ng/mL) and SB-505124 (10  $\mu$ M) for 48 hours. Cells were briefly trypsinized (3 minutes) and then were pelleted by centrifugation and washed 2 times with cold PBS. Cells were stained according to the manufacturer's recommendations (BD Pharmingen) using FITC annexin V in conjunction with propidium iodide, a vital dye. To set up compensation and quadrants, untreated cells were stained with FITC annexin V alone, with propidium iodide alone, or with both or left untreated. The cells were analyzed on a BD FACSCanto II system at the Baylor College of Medicine Flow Cytometry Core Facility. A total of 10 000 events were analyzed, and the statistical analysis was run on arcsine-transformed percentages of total cells.

### Cell cycle analysis

After the indicated treatment of COV434 cells,  $10^6$  single cells were washed twice in cold PBS, resuspended in 200  $\mu$ L of PBS, and fixed in 70% ethanol at –20°C overnight to resolve the sub-G<sub>1</sub> peak. Cells were pelleted and resuspended in a master mix containing propidium iodide (50  $\mu$ g/mL) and RNase (1 mg/mL). DNA content was analyzed on a BD FACSCanto II system, and the flow cytometry profiles were analyzed using BD FACSDiva software; 10 000 events were counted. G<sub>1</sub>, S, and G<sub>2</sub> phases are expressed as percentages of the cell population. Results were analyzed by FlowJo software using Dean-Jett-Fox modeling. The statistical analysis represents a comparison among normalized data values.

### Caspase 3/7 activity assay

COV434 cells were cultured in a 24-well plate at a density of  $5 \times 10^4$  cells/well and were left untreated as a control or were treated for 30 minutes with TGF $\beta$ 1 (2.5 ng/mL) alone, with SB-505124 (10  $\mu$ M) alone, or with a 30-minute pretreatment of SB-505124 (10  $\mu$ M) before TGF $\beta$ 1 addition. Caspase 3 and 7 activity was detected by adding a 1:1 ratio of Caspase-Glo 3/7 reagent (Promega). Cells were then mixed at 500 rpm for 30 seconds and incubated at room temperature for 2 hours. Background luminescence associated with the cell culture system and Caspase-Glo 3/7 reagent was subtracted from the experimental values. The luminescence of each sample was read on a luminometer (POLARstar Omega; BMG Labtech).

### Terminal deoxynucleotidyl transferase dUTP nick-labeling (TUNEL) assay

Apoptotic cells from control ovaries, *Smad1/5* dKO tumors, and *Smad1/5/4* tKO tumors and ovaries were assessed by the ApopTag Fluorescein In Situ Apoptosis Kit (Millipore). TUNEL-positive cells were imaged under an upright fluorescent microscope and defined as apoptotic cells. Tissues were counterstained with 4',6-diamidino-2-phenylindole (DAPI). TUNEL-pos-

itive cells were counted using a 40× objective lens on three randomly selected fields per section. A total of 2–3 nonadjacent sections per replicate (n = 3 mice per genotype) were analyzed.

## Statistical analysis

Statistical analysis was performed using GraphPad Prism 5 (GraphPad Software) or SPSS Statistics 22 (IBM). Multiple comparisons were performed using one-way ANOVA followed by a Tukey honestly significant difference (HSD) post hoc test. Percentage data from flow cytometric analysis and TUNEL assay experiments were arcsine transformed before statistical analysis to generate a normal distribution. Dose and time course response data were analyzed using a two-way ANOVA (time and treatment) and Tukey HSD test with logarithmic transformation of data. Unless otherwise stated, results were obtained from 3 independent experiments, carried out in duplicate or triplicate technical replicates.

## Results

### Deletion of *Smad4* from *Smad1/5* dKO mice caused sterility and increased atresia of developing follicles

Conditional deletion of *Smad1* and *Smad5* (*Smad1/5* dKO) from granulosa cells of the ovary causes reproductive dysfunction in female mice, and these mice are unable to reproduce after 4 to 6 months of age (7). In addition, *Smad1/5* dKO mice develop GCTs with full penetrance that show high levels of phosphorylated (ie, active) SMAD2/3 (7). The molecular and histologic profiles of these tumors are similar to those of human JGCTs (8), a rare form of ovarian cancer. To test the hypothesis that TGFβ-SMAD signaling plays a role in GCT development, we removed SMAD4-dependent signaling by deleting the common SMAD4 from the *Smad1/5* dKO mouse model. To do so, we crossed mice with loxP-flanked (“floxed”) alleles of *Smad4* (*Smad4<sup>fllox/flox</sup>*) (15) to the *Smad1<sup>fllox/flox</sup>Smad5<sup>fllox/flox</sup>Amhr2<sup>cre/+</sup>* mouse model (7) to generate a *Smad1<sup>fllox/flox</sup>Smad5<sup>fllox/flox</sup>Smad4<sup>fllox/flox</sup>Amhr2<sup>cre/+</sup>* triple conditional knockout (*Smad1/5/4* tKO). The *Amhr2cre* strain deletes floxed alleles in the ovary, oviduct, and uterus (27), and we found evidence of recombination in all three tissues (Supplemental Figure 1).

The fertility of mice conditionally null for *Smad1/5* dKO and *Smad4* is compromised, and both *Smad1/5* dKO and *Smad4* cKO mice have significantly reduced litter sizes compared with those of their controls (7, 15) (Figure 1A). In contrast, *Smad1/5/4* tKO mice are sterile (Figure 1A); in fertility studies of 6 breeding pairs allowed to mate for 6 months, *Smad1/5/4* female mice never produced a litter, even though vaginal plugs, indicating copulation, were seen. Previously, we reported that *Smad4* cKO mice have defects in follicle development, including

a significant increase in atretic preantral follicles and a reduced number of antral stage follicles (15). Therefore, we analyzed follicle development in the *Smad1/5/4* tKO ovaries. Compared with those of their control littermates, 12-week-old *Smad1/5/4* tKO ovaries had significantly more atretic follicles (Figure 1B). The increase in atretic follicles was similar to that in *Smad4* cKO ovaries (Figure 1B) (15). To verify that atretic follicles were dying by apoptosis, we further analyzed 12-week-old *Smad4* cKO and *Smad1/5/4* tKO ovaries by TUNEL assay. As expected, ovaries from *Smad4* cKO and *Smad1/5/4* tKO mice had increased granulosa cell apoptosis compared with those of their controls (Figure 1, D and F).

### Removal of *Smad4* from *Smad1/5* dKO mice increased survival and reduced GCT size and metastasis

*Smad4* cKO mice have lifespans similar to those of their controls, and no tumors develop in these mice (15). However, 100% of *Smad1/5* dKO (15 of 15) mice die within a 1-year time frame (7) (Figure 2A). Microscopic tumors in *Smad1/5* dKO mice are present by 8 weeks of age (7). In contrast, from the 1-year breeding study, only 1 of 8 (12.5%) *Smad1/5/4* tKO mice died; upon necropsy, there was an ovarian tumor present in that mouse (Figure 2E). Subsequent to the breeding study, 3 additional *Smad1/5/4* tKO mice in our colony developed GCTs, 1 of which was 18 months old, an age never attained by *Smad1/5* dKO females. Tumors from the *Smad1/5/4* tKO mice were much smaller in size than those of *Smad1/5* dKO mice (Figure 2E). *Smad1/5/4* tKO tumors were encapsulated and highly vascularized (Figures 2 and 3), but unlike the *Smad1/5* dKO mice, none of the *Smad1/5/4* tKO mice demonstrated peritoneal metastasis. Ovarian tumors from *Smad1/5/4* tKO mice were positive for inhibin α, a marker for GCTs (28) (Figure 3, D and F), and negative for the epithelial tumor markers cytokeratin 8 and 19 (data not shown).

Because *Smad4* cKO mice show defects in granulosa cell differentiation and increased levels of atretic follicles (15), we tested whether there was increased apoptosis in tumors of *Smad1/5/4* tKO mice. We analyzed the degree of apoptosis in double and triple knockout tumors by TUNEL assay and detected a significantly greater number of apoptotic cells in *Smad1/5/4* tKO tumors than in *Smad1/5* dKO tumors (Figure 3, G–I). These data suggested that loss of TGFβ signaling in GCTs via deletion of *Smad4* may reduce tumor aggressiveness by increasing granulosa cell apoptosis.

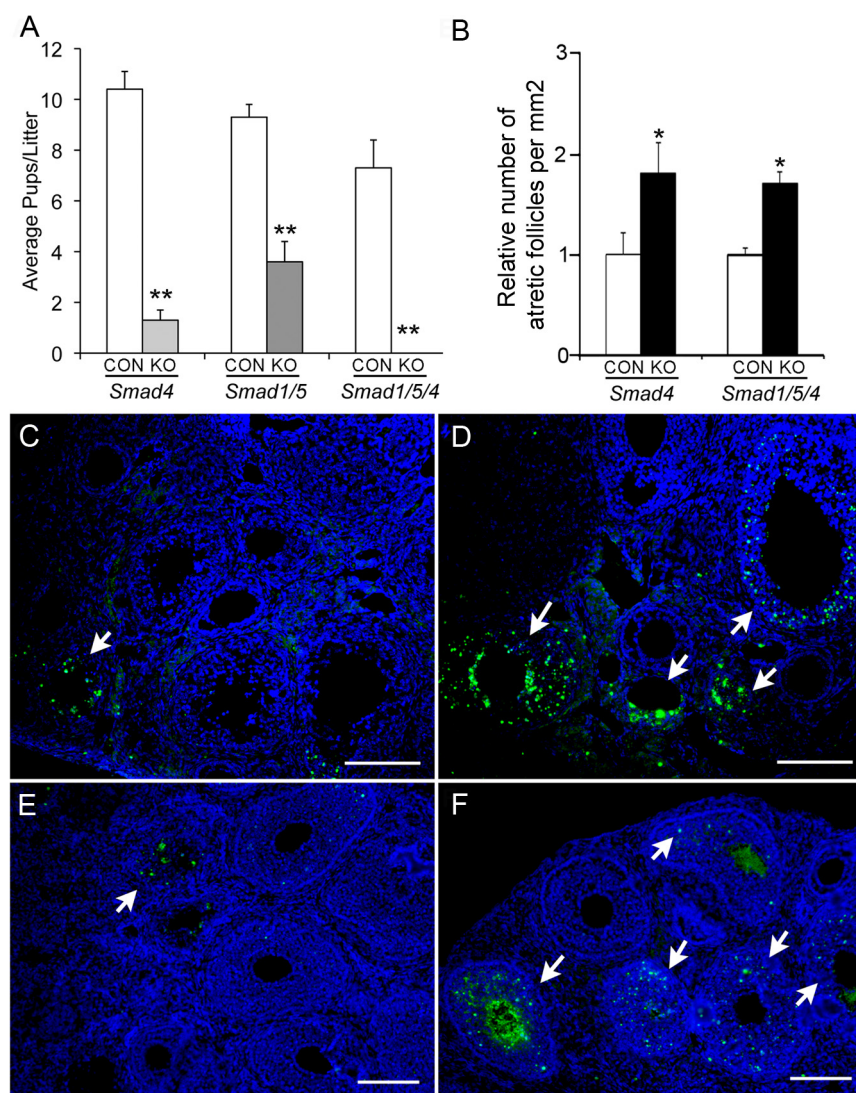


**Figure 1.** A, Fertility analysis of *Smad4* cKO, *Smad1/5* dKO, and *Smad1/5/4* tKO females. *Smad4* cKO ( $n = 7$ ) mice and their controls (CON,  $n = 7$ ) (15), *Smad1/5* dKO ( $n = 5$ ) mice and their controls ( $n = 5$ ), and *Smad1/5/4* tKO ( $n = 6$ ) mice and their controls ( $n = 6$ ) were bred continuously for 6 months and the numbers of pups per litter were recorded. Data are shown as mean pups per litter  $\pm$  SEM. \*\*,  $P < .01$  between the respective genotype and their controls. B, Numbers of atretic follicles per millimeter squared in ovaries of 12-week-old *Smad4* cKO and *Smad1/5/4* tKO mice compared with those of their respective control littermates. \*,  $P < .05$ . C–F, TUNEL analysis for apoptotic cells (green) in ovaries of 12-week-old *Smad4*<sup>flx/flx</sup> controls (C), *Smad4*<sup>flx/flx</sup>Amhr2<sup>cre/+</sup> females (D), *Smad1*<sup>flx/flx</sup>*Smad5*<sup>flx/flx</sup>*Smad4*<sup>flx/flx</sup> controls (E), and *Smad1*<sup>flx/flx</sup>*Smad5*<sup>flx/flx</sup>*Smad4*<sup>flx/flx</sup>Amhr2<sup>cre/+</sup> females (D). Arrows indicate atretic follicles. Nonspecific staining (visible in panel F) was detected in follicular antra (ns), and some dying oocytes with atretic cumulus cells are visible in *Smad1/5/4* dKO ovaries (asterisk). Ovaries were counterstained with DAPI (blue). Scale bar corresponds to 100  $\mu$ m.

### Expression levels of TGF $\beta$ and activin and their signaling components are altered in *Smad1/5* dKO GCT and are expressed in human JGCT samples

Both activin and TGF $\beta$  are able to signal through SMAD2/3, and active forms of SMAD2/3 (phospho-SMAD2/3) are found in mouse (*Inha*<sup>-/-</sup> and *Smad1/5* dKO) and human JGCTs (8). However, it is not known which TGF $\beta$  or activin isoforms or their receptors are expressed in JGCTs. Therefore, we first determined the

expression of these in both mouse and human samples of JGCTs.

From mice, we accessed the relative transcript levels in control pre-ovulatory granulosa cells and *Smad1/5* dKO tumor and metastasis samples by qPCR. All 3 TGF $\beta$  isoforms (*Tgfb1*, *Tgfb2*, and *Tgfb3*) and their receptors were detectable in tumor samples (Figure 4). Interestingly, we found that in the metastatic implants, there was evidence for up-regulation of the TGF $\beta$  signaling system: the *Tgfb3* isoform and the major TGF $\beta$  type I receptor, *Tgfb1* (*Alk5*), and type III accessory receptor, *Tgfb3* (betaglycan), were significantly up-regulated in these samples (Figure 4, C, E, and F). We additionally examined expression of these genes in samples of human JGCTs, which included 3 primary tumors, 1 metastatic implant, and a human cell line derived from a JGCT (COV434) (Supplemental Table 1). Although our sample sizes are small because of the rarity of JGCTs, all samples expressed at least one TGF $\beta$  isoform and the TGF $\beta$  type I and type II receptors (Figure 5). The type III receptor, *TGFBR3* (betaglycan), which was previously shown to be down-regulated in AGCTs (29), was also down-regulated in our JGCT samples (Figure 5F). There was one consistent outlying JGCT sample, which was derived from a metastatic implant from a 15-year-old patient with a stage IIIC malignant JGCT. Mean values for this sample were generally greater than those for the others (Figure 5, red boxes). Interestingly, both the

mouse *Smad1/5* dKO and the human metastatic sample showed up-regulation of *TGFBR3*, *TGFBR1*, and *TGFBR3*, suggesting that the TGF $\beta$  system may be up-regulated during metastatic progression in both mouse and human JGCTs.

Activins induce SMAD2/3 phosphorylation through activation of the activin receptor type II (ACVR2A and ACVR2B) and activin type 1B (ACVR1B; also called ALK4) receptor complexes, and activin signaling has been

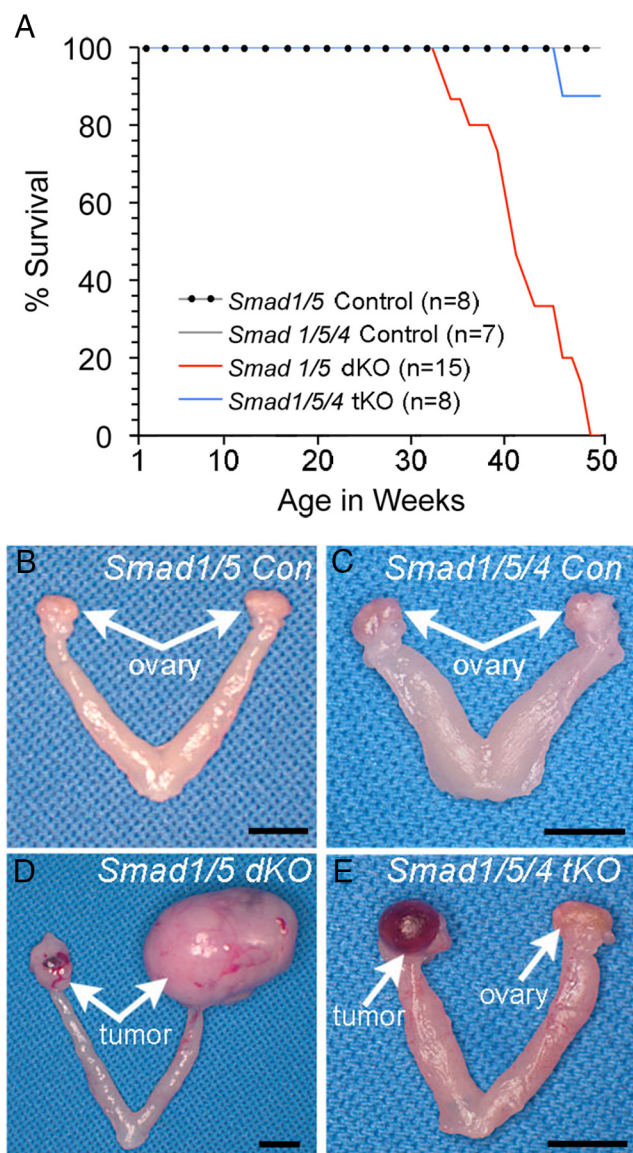


**Figure 2.** Genetic deletion of *Smad4* delays tumor development in *Smad1/5* dKO mice. A, Survival curve for *Smad1*<sup>flx/flx</sup>*Smad5*<sup>flx/flx</sup> (*Smad1/5* control; n = 8), *Smad1*<sup>flx/flx</sup>*Smad5*<sup>flx/flx</sup>*Amhr2*<sup>cre/+</sup> (*Smad1/5* dKO; n = 15), *Smad1*<sup>flx/flx</sup>*Smad5*<sup>flx/flx</sup>*Smad4*<sup>flx/flx</sup> (*Smad1/5/4* control; n = 7), and *Smad1*<sup>flx/flx</sup>*Smad5*<sup>flx/flx</sup>*Smad4*<sup>flx/flx</sup>*Amhr2*<sup>cre/+</sup> (*Smad1/5/4* tKO; n = 8). Of *Smad1/5* dKO mice, 100% died within 1 year, whereas only 12.5% of the *Smad1/5/4* tKO mice died within the same time frame (1 of 8). B–E, Gross morphology of ovarian tumors in *Smad1/5* dKO (D) and *Smad1/5/4* tKO (E) mice at 6 months. Note that the size of the *Smad1/5/4* tKO tumor (E) is similar to that of the control ovary (C), whereas the *Smad1/5* dKO tumor is much larger (D). Scale bar corresponds to 5 mm.

implicated in GCT progression in mice (13, 30). To determine whether the activin signaling components were also present in *Smad1/5* dKO tumors, we quantified expression of activin subunits ( $\beta$ A [*Inhba*] and  $\beta$ B [*Inhbb*]), the type II receptors (*Acvr2a* and *Acvr2b*), and the type I receptor (*Acvr1b*) in healthy granulosa cells and *Smad1/5* dKO tumor and metastasis samples (Supplemental Figure 2). *Inhba* and *Inhbb* were significantly down-regulated in

both tumors and metastasis samples compared with those in control granulosa cells (Supplemental Figure 2, A and B). All of the activin receptors were expressed, and the type II receptor, *Acvr2a*, and type I receptor, *Acvr1b*, increased in metastasis samples (Supplemental Figure 2, C and E). Human JGCTs also express *INHBA* and *INHBB*, as well as the activin receptors (Supplemental Figure 3). In general, the mean levels of the activin receptors, *ACVR2A*, *ACVR2B*, and *ACVR1B*, were not statistically different from those in the ovary (Supplemental Figure 3).

### TGF $\beta$ 1 repressed apoptosis in the human JGCT cell line, COV434

Few studies have examined TGF $\beta$  signaling in primary samples of JGCTs (8), and there are only limited studies on the effects of the TGF $\beta$ 2 isoform in the human JGCT cell line, COV434 (29, 31). Therefore, to further examine the role of TGF $\beta$  in JGCTs, we treated COV434 cells with recombinant human (rh) TGF $\beta$ 1 or with SB-505124 (a small molecule inhibitor of the TGF $\beta$  family type I receptors that signal through SMAD2/3 [ALK4/5/7] but not SMAD1/5/8 [ALK1/2/3/6]) (20, 21) and monitored cell proliferation for 72 hours. Treatment with TGF $\beta$ 1 caused a statistically significant increase in the number of viable cells compared with those for the control (Figure 6A). Incubation with SB-505124 caused a significant decline in the number of viable cells, indicating that ALK4/5/7 are constitutively active in the COV434 cell line, as suggested by the expression data (Figure 5). Furthermore, the inhibition by SB-505124 cannot be overcome by exogenously adding additional TGF $\beta$ . These results indicate that activation of a TGF $\beta$ /activin receptor complex is required for COV434 cell survival.

TGF $\beta$  may promote cell survival through positive regulation of the cell cycle or, alternatively, through inhibition of apoptosis. Exogenous TGF $\beta$ 1 treatment or repression of endogenous TGF $\beta$ /activin signaling with SB-505124 did not alter the cell cycle as measured by flow cytometric analysis of DNA cell content using propidium iodide DNA staining (Supplemental Figure 4). Furthermore, small tumors from *Smad1/5/4* tKO mice showed increased apoptosis (Figure 3, G–I), suggesting that loss of TGF $\beta$  signaling by deletion of SMAD4 increased apoptosis. Therefore, we examined apoptosis in COV434 cells by propidium iodide-annexin V double labeling to detect phosphatidylserine externalization, a hallmark of the early phase of apoptosis by flow cytometry. This assay showed that inhibition with SB-505124 alone or with exogenous TGF $\beta$  increased apoptosis (Figure 6B and Supplemental Figure 5).

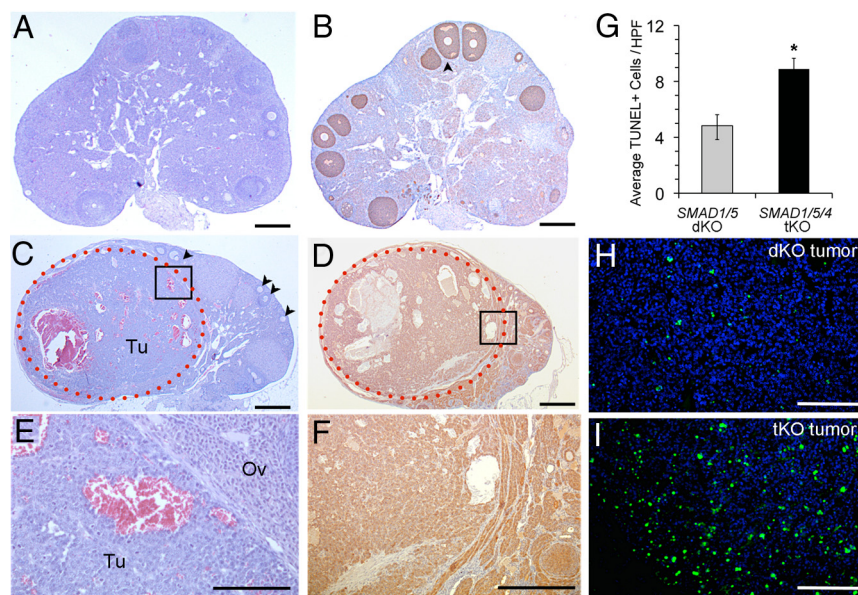


**Figure 3.** Histologic and TUNEL analysis of GCTs in *Smad1/5/4* tKO compared with *Smad1/5* dKO mice. A and B, Control ovaries showed no sign of tumor lesions (A) and granulosa cells are positive for inhibin  $\alpha$  immunoreactivity in growing follicles (B). C, Ovary from a 6-month-old *Smad1/5/4* tKO mouse showed a small encapsulated tumor (Tu), approximately the size of a normal ovary (Figure 1E), which is highly vascularized with strong immunoreactivity for inhibin  $\alpha$ , typical of GCTs (D and F). Arrowheads indicate follicles. E and F, higher magnifications of C and D, respectively. Ov, ovary. G, Quantification of TUNEL-positive cells in samples of *Smad1/5* dKO (n = 3) and *Smad1/5/4* tKO tumors (n = 3). A Fisher *t* test was used to assess significance between groups: \*, *P* < .05. HPF, high-power field. H, Representative TUNEL stain for a *Smad1/5* dKO tumor (FITC, apoptotic cells [green]; cells counterstained with DAPI [blue] to show cell nuclei). Many more apoptotic cells (green) are seen in *Smad1/5/4* tKO mice (I) compared with *Smad1/5* dKO (H) mice. Scale bars correspond to 200  $\mu$ m (A–D); 50  $\mu$ m (E and F); 100  $\mu$ m (H and I).

### TGF $\beta$ 1, but not activin A, inhibited caspase 3/7 activity and PARP1 cleavage

Caspase 3 plays a central role in the execution of apoptosis and is mainly responsible for the cleavage of PARP during cell death (32). To further explore the mechanisms of TGF $\beta$ 1 repression of apoptosis, we measured caspase 3 and caspase 7 activity in COV434 cells that were treated with TGF $\beta$ 1, the inhibitor SB-505124, or a combination of both. As expected, TGF $\beta$ 1 induced phospho-SMAD2/3 within 30 minutes of treatment (Figure 7C). In the same time frame, exogenous TGF $\beta$ 1 decreased caspase 3/7 activity by 50% compared with that in control-treated cells or in cells treated with the inhibitor alone (Figure 7A). Caspase 3/7 activity was restored to control levels when cells were preincubated with SB-505124 30 minutes before TGF $\beta$ 1 treatment (Figure 7A). Consistent with these data, immunoblot analysis revealed that exogenous TGF $\beta$ 1 repressed PARP1 cleavage compared with that in control-treated cells (Figure 7, C and E), with no effect on the endogenous levels of PARP1. Pretreatment with SB-505124 before TGF $\beta$ 1 incubation restored PARP1 degradation (Figure 7, C and E).

Because SB-505124 is an inhibitor of ALK4/5/7, it is also able to inhibit activin activity. Therefore, we determined whether activin showed the same inhibition of PARP1 cleavage as TGF $\beta$ 1. We used rh activin A alone, its antagonist follistatin alone, or a combination of both and analyzed apoptosis in COV434 cells. In contrast to TGF $\beta$ 1, caspase 3/7 activity was not regulated when COV434 cells were treated with activin A alone or in combination with follistatin (Figure 7B); however, follistatin alone was able to induce a 50% reduction in caspase activity (Figure 7B). Whereas immunoblot analysis showed that activin A induced SMAD2/3 phosphorylation in COV434 cells within 30 minutes, it did not regulate PARP1 activity as shown by the maintenance of the cleaved fragment, alone or in combination with follistatin (Figure 7, D–F). These results confirm the specific requirement of active TGF $\beta$  signaling leading to SMAD2/3 phosphorylation to inhibit apoptosis and a divergence of activity between TGF $\beta$  and activin even though both utilize SMAD2/3.

## Discussion

### TGF $\beta$ promotes tumorigenesis of JGCTs

Ovarian JGCTs are a rare gynecologic neoplasm with nearly 80% occurring within the first 2 decades of life (2). AGCTs have been more extensively studied than JGCTs, and a single somatic missense mutation in *FOXL2* in AGCT has been identified (6). In contrast, relatively little is known about the molecular mechanisms giving rise to JGCTs. Various TGF $\beta$  family members are known to play a key role in regulating granulosa cell proliferation and differentiation during folliculogenesis (33–35), and gain-of-function in activin activity through loss of *Inha* causes GCT development in mice (9, 10).

A previous study showed that a reduction in expression of the type III TGF $\beta$  receptor, *TGFBR3* (betaglycan), contributes to GCT development, although this study was done mostly on the adult form of the disease and in the COV434 cell line (29). However, COV434 cells show little sensitivity to the TGF $\beta$ 2 isoform (29). This is likely

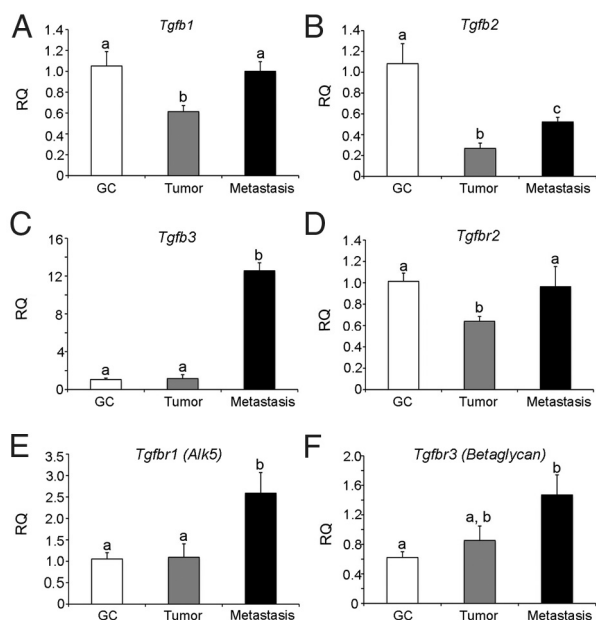


**Figure 4.** Expression of TGFβ ligands and receptors in *Smad1/5* dKO tumors and metastases. RNA was collected from granulosa cells (GC) of control mice ( $n = 6$ ), *Smad1/5* dKO tumors ( $n = 9$ ), and metastasis samples ( $n = 7$ ) mainly collected from tumor implants on the diaphragm. The relative quantity (RQ) of mRNA levels for *Tgfb1* (A), *Tgfb2* (B), *Tgfb3* (C), *Tgfb2* (D), *Tgfb1* (*Alk5*) (E), and *Tgfb3* (*Betaglycan*) (F) is shown. Fold change is expressed in arbitrary units relative to the mean of the control samples. *Gapdh* was used as a housekeeping gene to normalize samples. Statistical analysis was performed by ANOVA and the Tukey HSD test. Data are means  $\pm$  SEM. Statistical differences between means are indicated by different letters above the bars (ie, a is statistically different from b and c, but not a,b).

because TGFβ2 has a low affinity for the type II receptor (36, 37) and thus requires TGFBR3 to signal (38). In our study, we found that all of our primary JGCT samples express the 3 TGFβ ligands (*Tgfb1*, *Tgfb2*, and *Tgfb3*), and thus, TGFβ1 and TGFβ3 could compensate for the lack of TGFβ2 signaling in JGCTs, perhaps in contrast to AGCTs. We used TGFβ1 to study JGCT development, which (similar to TGFβ3) has a much higher (1000-fold) affinity for the TGFβ type II receptor, even in the absence of TGFBR3 (28, 39). We show that a gain in TGFβ activity that occurs with the loss of the BMP SMADs (SMAD1 and SMAD5) results in suppression of apoptosis and promotes increased survival of tumor cells, both in vitro using a human JGCT cell line and in vivo by deleting *Smad4* from the *Smad1/5* dKO.

### TGFβ promotes juvenile granulosa cell tumorigenesis by inhibiting apoptosis

Cellular homeostasis is a result of a balance between cell proliferation, differentiation, and apoptosis and is regulated by multiple signaling molecules and growth factors including members of TGFβ signaling pathway. Cancer may result from a disruption of this balance, tipping it

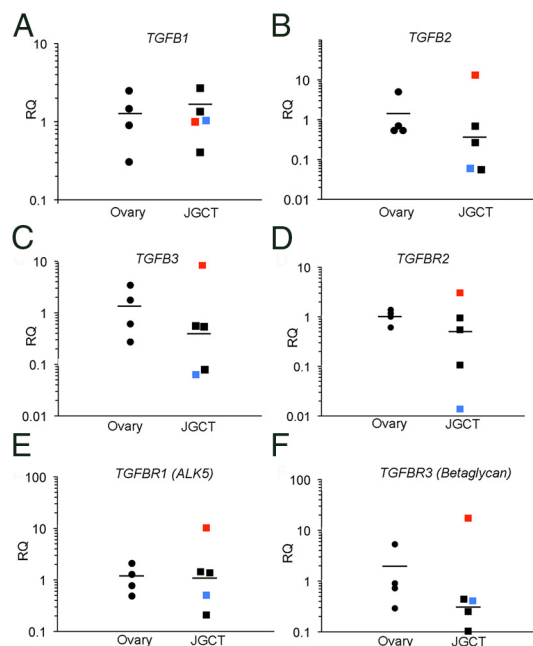


**Figure 5.** TGFβ ligands and receptors in human JGCTs. RNA was collected from healthy ovaries from premenopausal women ( $n = 4$ ), human JGCTs ( $n = 4$ ), and control COV434 cell samples (mean of  $n = 6$  samples shown as a single blue box). The relative quantity (RQ) of mRNA levels of *TGFβ1* (A), *TGFβ2* (B), *TGFβ3* (C), *TGFβ2* (D), *TGFBR1* (*ALK5*) (E), and *TGFBR3* (*Betaglycan*) (F) are shown. Fold change is expressed in arbitrary units relative to the mean of the control samples. The mean of each group is shown by a horizontal bar. The mean of the JGCT samples was calculated excluding the outlying JGCT sample (red box) and the COV434 cells (blue box). *GAPDH* was used as a housekeeping gene to normalize samples. The outlying JGCT sample (red box) was obtained from implant from a patient with stage IIIc malignant JGCT (Supplemental Table 1; sample 1).

in favor of growth (40). Our results demonstrate that a small molecule inhibitor of TGFβ signaling such as SB-505124, which blocks signaling from the type I receptors ALK4/5/7 but not from the other type I receptors (ALK1/2/3/6), increases apoptosis in COV434 cells, whereas rh TGFβ1 represses it. We further showed that TGFβ1 represses caspase 3/7 activity and PARP1 cleavage. Even though activin A also utilizes SMAD2 and SMAD3 as does TGFβ1, it has no effect on the caspases in COV434 cells and, therefore, on PARP1 cleavage. Caspases are considered to be the major executor of apoptosis (32). The effector caspases (3, 6, and 7) target several proteins, among which are the PARP proteins, which have been implicated in genomic stability maintenance by responding to DNA damage (40, 41). Once PARP is cleaved by caspase 3, it no longer exerts its inhibition on the DNASE1L3 endonuclease activity, which ultimately leads to cell death (41). Taken together, our data suggest that TGFβ regulates PARP1 cleavage and the apoptotic process in JGCTs.

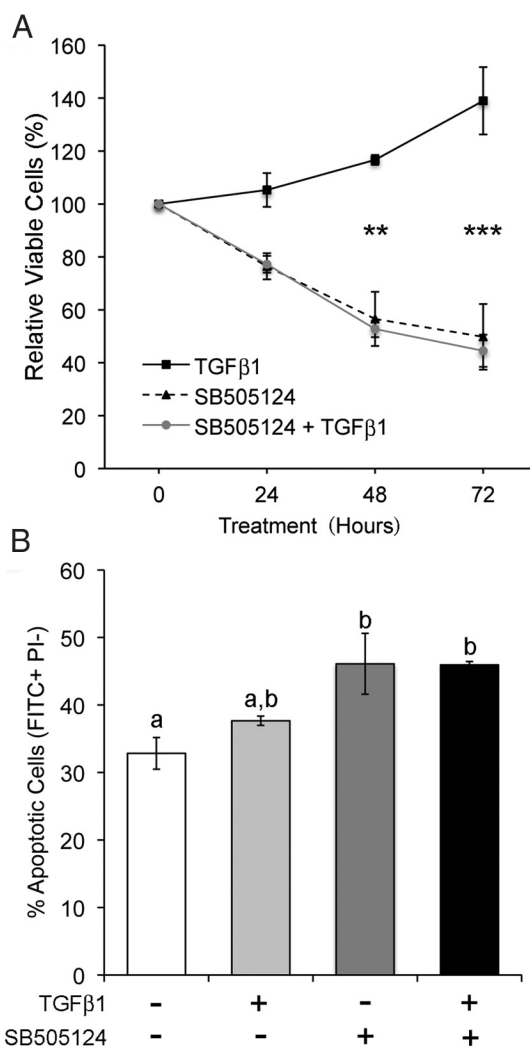


**Figure 6.** Effects of TGFβ and its inhibition on a human JGCT cell line, COV434, for cell viability and apoptosis. A, Subconfluent COV434 cells were treated with TGFβ1 (2.5 ng/mL), SB-505124 (10 μM), or a combination of the 2 and assayed by MTS at 24, 48, and 72 hours. Each point represents the mean ± SEM of 3 independent experiments performed in duplicate, relative to the control-treated cells. Data were log transformed and analyzed by two-way ANOVA and the Tukey HSD test. Statistical significances between treatment groups at the same time point: \*\*,  $P < .01$  between TGFβ1- and SB-505124-treated groups at 48 hours; \*\*\*,  $P < .001$  between TGFβ1- and SB-505124-treated samples at 72 hours. B, Subconfluent COV434 cells were treated for 72 hours as above, but stained with annexin V and propidium iodide (PI) and assayed using flow cytometry. The means ± SEM of 3 independent experiments are shown. Different letters within each category (viable cells, early and late apoptosis) indicate statistical significance ( $P < .05$ ) by ANOVA and the Tukey HSD test on transformed data.

### Activin and TGFβ may have separable roles in GCT

GCTs that develop in both *Smad1/5* dKO mice and *Inha* KO mice, as well as samples of human JGCTs, show evidence of activated SMAD2/3 (7, 8). SMAD2/3 are phosphorylated in response to TGFβ family ligands that bind to the type I receptors, ACRVR1B (ALK4), TGFBR1 (ALK5), and ACVR1C (ALK7), including the activins

and TGFβs. All *Inha*<sup>-/-</sup> mice develop GCTs and die from a cancer cachexia-like syndrome that is dependent on signaling from systemic activin produced from the tumors (9, 30). In contrast, *Smad1/5* dKO mice do not develop cancer cachexia, even though all mice develop GCTs, suggesting that activin is not highly secreted from the tumors. In addition, we found that the activin subunits were significantly down-regulated in *Smad1/5* dKO tumors. This finding coupled with the high level of expression of *Inha* in the *Smad1/5* dKO tumors and the increased inhibins in the serum suggests that inhibin may be formed preferentially over activin in *Smad1/5* dKO mice (8, 42). The high levels of inhibin may further antagonize any local effects of activin (42–44). By measuring caspase activity in COV434 cells treated with activin alone or in combination with follistatin, we reported no effect of activin A on caspase 3/7 activity, and concomitantly, a maintenance of PARP1 integrity. Nevertheless, we found that follistatin alone shows an effect on caspase 3/7 activity remains unclear, as TGFβ ligands are not inhibited by follistatin (36–38), although some BMPs can be (45). In total, however, these experiments suggest that activin signaling does not play a key role in regulating the apoptosis process in COV434 cells or in *Smad1/5* dKO GCTs. These results provide evidence that it is probably TGFβ signaling that allows tumor progression by suppressing apoptosis. Additional contributions of activin to JGCT development may also occur because COV434 cells appear to be fully able to phosphorylate SMAD2/3 when exposed to exogenous activin A.

### SMAD4 loss modifies GCT apoptosis

Inhibition of TGFβ signaling by targeting the TGFβ family type I receptor with small inhibitory molecules could potentially also inhibit noncanonical pathway signaling. To demonstrate the role of the canonical TGFβ-SMAD pathway in *Smad1/5* dKO tumor development, we generated a triple knockout mice model for *Smad1*, *Smad4*, and *Smad5*, namely *Smad1/5/4* tKO. Although SMAD2 and SMAD3 mutations are relatively rare in cancer (46, 47), SMAD4 inactivation is commonly found in gastric, pancreatic, and colorectal cancer and less frequently in breast, ovarian, and lung tumors (48–51). Our model for the role of *Smad4* in *Smad1/5* tumorigenesis is complicated by the stochastic nature of recombination and the functional redundancy between *Smad1* and *Smad5* (7). In mice, *Smad4* conditional deletion in preantral or preovulatory granulosa cells does not give rise to tumors but leads to infertility and an increase in atretic follicles (15, 52). In the *Smad1/5/4* tKO model, recombination of both alleles of *Smad4* before *Smad1* and *Smad5*

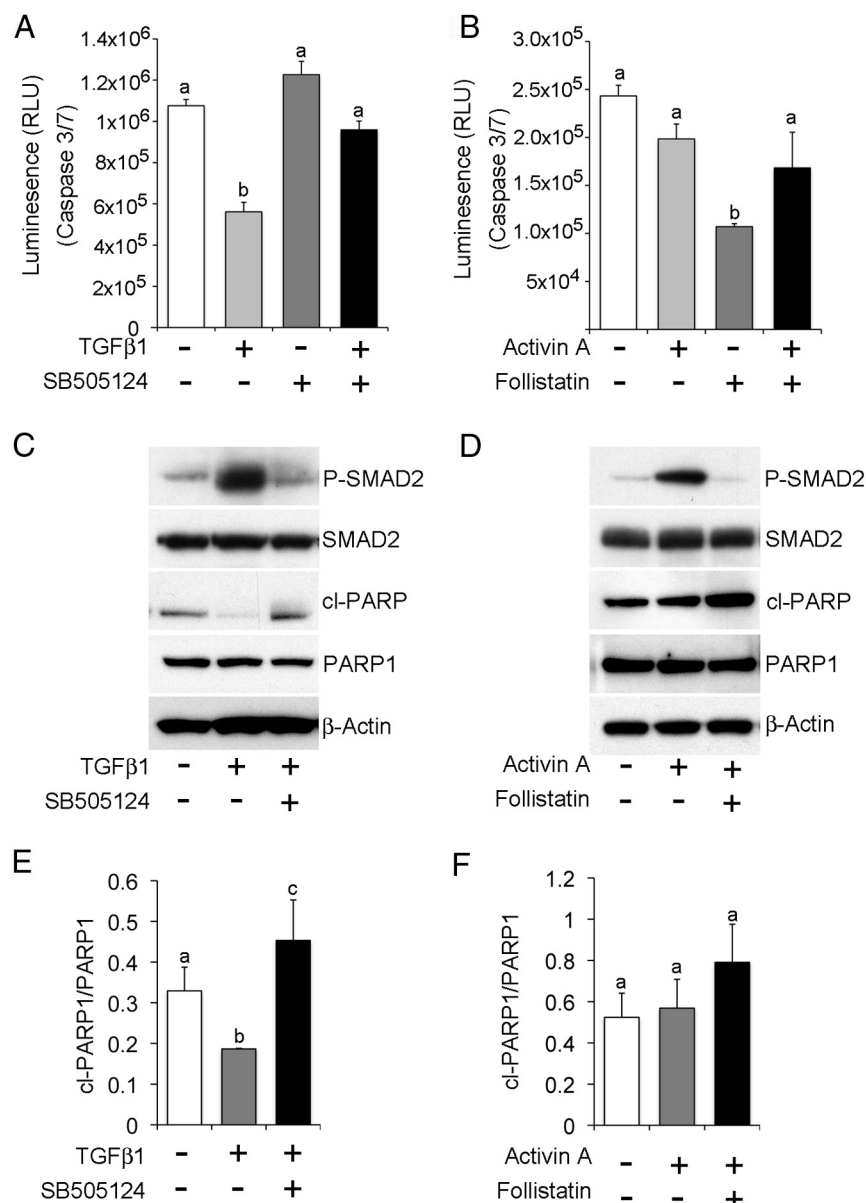


**Figure 7.** TGFβ1 inhibits caspase 3/7 activity and prevents PARP1 cleavage. A, COV434 cells were treated with vehicle (control), TGFβ1 (2.5 ng/mL), SB-505124 (10 μM), or a combination of TGFβ1 (2.5 ng/mL) and SB-505124 (10 μM) for 30 minutes. Cells were assayed for caspase 3 and 7 activity by a luminescence assay. Units are expressed as relative luminescence units (RLU) ± SEM from three independent experiments assayed in triplicate. Results are presented as means ± SEM. B, COV434 cells were treated with vehicle (control), activin A (25 ng/mL), follistatin (400 ng/mL), or a combination of activin A (25 ng/mL) and follistatin (400 ng/mL) for 30 minutes and then were assayed for caspase 3 and 7 activity by a luminescence assay. Units are expressed as relative luminescence units ± SEM from 3 independent experiments assayed in triplicate. Results are presented as means ± SEM. C and D, Immunoblot analysis of COV434 cells that were treated as indicated. Cell lysates were immunoblotted with anti-phospho (P)-SMAD2/3, anti-total SMAD2, anti-cleaved (cl) PARP1, anti-total PARP1, or anti-β-actin antibodies. E and F, Quantification of 3 independent immunoblots for cl-PARP1/PARP1. Statistical analysis of all panels is presented by different letters above the bars that indicate statistically different means by ANOVA and the Tukey HSD test ( $P < .05$ ) (ie, a is statistically different from b and c).

could result in loss of granulosa cells before tumor formation, which may be one reason that the tumors develop more slowly. Even so, these data further highlight the importance of the SMAD4 pathway in maintaining the

viability of granulosa cells (15, 52). However, when *Smad1/5/4* tKO tumors arise, they are less aggressive. In this case, recombination of *Smad1* and *Smad5* before loss of *Smad4* probably allows tumors to form, and loss of *Smad4* then appears to restrain tumor growth by tipping the balance toward apoptosis. In addition, we did not observe metastatic tumor development in the *Smad1/5/4* tKO mice, suggesting that the aggressiveness of JGCTs requires TGFβ signaling through SMAD4. In support of a role for TGFβ in GCT tumor progression to metastasis in mice, the *Tgfb3* isoform, the type I receptor, *Tgfb1*, and the type III receptor, *Tgfb3*, are significantly increased in metastasis samples and the single sample of a JGCT implant that we were able to obtain had similar increases in ligands and receptors.

SMAD4, part of the activated trimeric SMAD transcription factor complex, is a crucial player in TGFβ signaling and has been shown to mediate expression of a large number of downstream targets in both normal epithelial and cancer cells (53, 54). In granulosa cells, loss of *Smad4* causes endocrine disorders in both murine and porcine models and induces a dramatic effect on the number of viable granulosa cells (15, 52, 55). In porcine models, SMAD4 modulates granulosa cell proliferation by regulating cell cycle factors such as cyclin D2, whereas in mice *Smad4* conditional deletion leads to more atretic follicles by inducing apoptosis (15, 52, 56). However, the mechanism by which SMAD4 mediates apoptosis in mouse or human granulosa cells or their tumors remains to be determined. The suppression of apoptosis

by SMAD4 in granulosa cells may be a direct effect, for example, by regulation of a key gene involved in apoptosis, or an indirect event, for example, by SMAD4 regulation of a key growth factor for granulosa cell survival.

BAX is a known target gene of TGF $\beta$ , although its regulation (up or down) is cell type dependent (57–60). Alternatively, microRNAs (small noncoding RNAs that regulate gene expression at posttranscriptional levels) could play a role in SMAD4-mediated apoptosis, and it has been shown in granulosa cells that microRNA-224 is a SMAD4 target gene that promotes granulosa cell proliferation (61). The involvement of microRNA-224 in apoptosis repression was also recently shown in hepatocellular carcinoma (62), and a similar mechanism may occur in GCT development. Thus, to fully understand the role of SMAD4 in GCT development, a further analysis of its activity in granulosa cells or their tumors is warranted.

In conclusion, our present study demonstrates that TGF $\beta$  provides a protective signal in mouse and human JGCTs, preventing them from undergoing apoptosis, which ultimately enhances tumor development. These results show that GCT survival in *Smad1/5* dKO mice can be sustained by endogenous TGF $\beta$  signaling and provide evidence that inhibition of TGF $\beta$ RI/ALK5 in human GCTs leads to prevention of tumor progression by the induction of cell apoptosis. Thus, the use of specific small molecule inhibitors directed against TGF $\beta$  might be of specific interest for clinical application in juvenile GCTs.

## Acknowledgments

We thank Drs. Elizabeth Robertson (University of Oxford, Oxford, United Kingdom) for the *Smad1* and *Smad4* mice, Richard Behringer (University of Texas M. D. Anderson Cancer Center, Houston, Texas) for the *Amhr2cre* mice, and An Zwijsen and Lieve Umans (University of Leuven, Leuven, Belgium) for the *Smad5* floxed mice.

Address all correspondence and requests for reprints to: Stephanie A. Pangas, PhD, Department of Pathology and Immunology, Department of Molecular and Cellular Biology, Baylor College of Medicine, One Baylor Plaza, Houston, TX 77030. E-mail: [spangas@bcm.edu](mailto:spangas@bcm.edu).

This project was supported by the Human Tissue Acquisition and Pathology Core at Baylor College of Medicine with funding from the National Institutes of Health (Grant P30 CA125123), by the Cytometry and Cell Sorting Core at Baylor College of Medicine with funding from the National Institutes of Health (Grants AI036211, CA125123, and RR024574) and the expert assistance of Joel M. Sederstrom, by the National Institutes of Health (Grant R01 CA138628), by a Burroughs Wellcome Career Award in the Biomedical Sciences, and by a Susan Poorman Blackie Ovarian Cancer Foundation grant (to S.A.P.).

Disclosure Summary: The authors have nothing to disclose.

## References

- Schumer ST, Cannistra SA. Granulosa cell tumor of the ovary. *J Clin Oncol*. 2003;21:1180–1189.
- Young RH, Dickersin GR, Scully RE. Juvenile granulosa cell tumor of the ovary. A clinicopathological analysis of 125 cases. *Am J Surg Pathol*. 1984;8:575–596.
- Jamieson S, Butzow R, Andersson N, et al. The FOXL2 C134W mutation is characteristic of adult granulosa cell tumors of the ovary. *Mod Pathol*. 2010;23:1477–1485.
- Greenacre CB. Spontaneous tumors of small mammals. *Vet Clin North Am Exot Anim Pract*. 2004;7:627–651, vi.
- Liebelt AG, Sass B, Lombard LS. Mouse ovarian tumors—a review including classification and induction of neoplastic lesions and description of several previously unreported types. *J Exp Pathol*. 1987;3:115–145.
- Shah SP, Köbel M, Senz J, et al. Mutation of FOXL2 in granulosa-cell tumors of the ovary. *N Engl J Med*. 2009;360:2719–2729.
- Pangas SA, Li X, Umans L, et al. Conditional deletion of Smad1 and Smad5 in somatic cells of male and female gonads leads to metastatic tumor development in mice. *Mol Cell Biol*. 2008;28:248–257.
- Middlebrook BS, Eldin K, Li X, Shivasankaran S, Pangas SA. Smad1-Smad5 ovarian conditional knockout mice develop a disease profile similar to the juvenile form of human granulosa cell tumors. *Endocrinology*. 2009;150:5208–5217.
- Coerver KA, Woodruff TK, Finegold MJ, Mather J, Bradley A, Matzuk MM. Activin signaling through activin receptor type II causes the cachexia-like symptoms in inhibin-deficient mice. *Mol Endocrinol*. 1996;10:534–543.
- Matzuk MM, Finegold MJ, Su JG, Hsueh AJ, Bradley A.  $\alpha$ -Inhibin is a tumour-suppressor gene with gonadal specificity in mice. *Nature*. 1992;360:313–319.
- Shi Y, Massagué J. Mechanisms of TGF- $\beta$  signaling from cell membrane to the nucleus. *Cell*. 2003;113:685–700.
- Massagué J. TGF $\beta$  signalling in context. *Nat Rev Mol Cell Biol*. 2012;13:616–630.
- Li Q, Graff JM, O'Connor AE, Loveland KL, Matzuk MM. SMAD3 regulates gonadal tumorigenesis. *Mol Endocrinol*. 2007;21:2472–2486.
- Hill CS. Nucleocytoplasmic shuttling of Smad proteins. *Cell Res*. 2009;19:36–46.
- Pangas SA, Li X, Robertson EJ, Matzuk MM. Premature luteinization and cumulus cell defects in ovarian-specific Smad4 knockout mice. *Mol Endocrinol*. 2006;20:1406–1422.
- Nagaraja AK, Middlebrook BS, Rajanahally S, et al. Defective gonadotropin-dependent ovarian folliculogenesis and granulosa cell gene expression in inhibin-deficient mice. *Endocrinology*. 2010;151:4994–5006.
- Cheng G, Weihua Z, Mäkinen S, et al. A role for the androgen receptor in follicular atresia of estrogen receptor  $\beta$  knockout mouse ovary. *Biol Reprod*. 2002;66:77–84.
- Hu YC, Wang PH, Yeh S, et al. Subfertility and defective folliculogenesis in female mice lacking androgen receptor. *Proc Natl Acad Sci USA*. 2004;101:11209–11214.
- Tripurani SK, Cook RW, Eldin KW, Pangas SA. BMP-specific SMADs function as novel repressors of PDGFA and modulate its expression in ovarian granulosa cells and tumors. *Oncogene*. 2013;32:3877–3885.
- DaCosta Byfield S, Major C, Laping NJ, Roberts AB. SB-505124 is a selective inhibitor of transforming growth factor- $\beta$  type I receptors ALK4, ALK5, and ALK7. *Mol Pharmacol*. 2004;65:744–752.
- Vogt J, Traynor R, Sapkota GP. The specificities of small molecule inhibitors of the TGF $\beta$  and BMP pathways. *Cell Signal*. 2011;23:1831–1842.
- Wu TH, Chou YW, Chiu PH, Tang MJ, Hu CW, Yeh ML. Validation of the effects of TGF- $\beta$ 1 on tumor recurrence and prognosis through tumor retrieval and cell mechanical properties. *Cancer Cell Int*. 2014;14:20.
- Remst DE, Blaney Davidson EN, Vitters EL, et al. TGF- $\beta$  induces

- lysyl hydroxylase 2b in human synovial osteoarthritic fibroblasts through ALK5 signaling. *Cell Tissue Res.* 2014;355:163–171.
24. Von Zee CL, Langert KA, Stubbs EB Jr. Transforming growth factor- $\beta$  induces synthesis and secretion of endothelin-1 in human trabecular meshwork cells. *Invest Ophthalmol Vis Sci.* 2012;53:5279–5286.
25. Buckley S, Shi W, Barsky L, Warburton D. TGF- $\beta$  signaling promotes survival and repair in rat alveolar epithelial type 2 cells during recovery after hyperoxic injury. *Am J Physiol Lung Cell Mol Physiol.* 2008;294:L739–L748.
26. Noma K, Smalley KS, Lioni M, et al. The essential role of fibroblasts in esophageal squamous cell carcinoma-induced angiogenesis. *Gastroenterology.* 2008;134:1981–1993.
27. Jamin SP, Arango NA, Mishina Y, et al. Requirement of Bmpr1a for Müllerian duct regression during male sexual development. *Nat Genet.* 2002;32:408–410.
28. Cheifetz S, Hernandez H, Laiho M, ten Dijke P, Iwata KK, Massagué J. Distinct transforming growth factor- $\beta$  (TGF- $\beta$ ) receptor subsets as determinants of cellular responsiveness to three TGF- $\beta$  isoforms. *J Biol Chem.* 1990;265:20533–20538.
29. Bilandzic M, Chu S, Farnworth PG, et al. Loss of betaglycan contributes to the malignant properties of human granulosa tumor cells. *Mol Endocrinol.* 2009;23:539–548.
30. Li Q, Kumar R, Underwood K, et al. Prevention of cachexia-like syndrome development and reduction of tumor progression in inhibin-deficient mice following administration of a chimeric activin receptor type II-murine Fc protein. *Mol Hum Reprod.* 2007;13:675–683.
31. Bilandzic M, Chu S, Wang Y, et al. Betaglycan alters NF $\kappa$ B-TGF $\beta$ 2 cross talk to reduce survival of human granulosa tumor cells. *Mol Endocrinol.* 2013;27:466–479.
32. Cohen GM. Caspases: the executioners of apoptosis. *Biochem J.* 1997;326(Pt 1):1–16.
33. Findlay JK, Drummond AE, Dyson ML, Baillie AJ, Robertson DM, Ethier JF. Recruitment and development of the follicle; the roles of the transforming growth factor- $\beta$  superfamily. *Mol Cell Endocrinol.* 2002;191:35–43.
34. Pangas SA. Bone morphogenetic protein signaling transcription factor (SMAD) function in granulosa cells. *Mol Cell Endocrinol.* 2012;356:40–47.
35. Myers M, Pangas SA. Regulatory roles of transforming growth factor  $\beta$  family members in folliculogenesis. *Wiley Interdiscip Rev Syst Biol Med.* 2010;2:117–125.
36. Thompson TB, Lerch TF, Cook RW, Woodruff TK, Jardtetzky TS. The structure of the follistatin:activin complex reveals antagonism of both type I and type II receptor binding. *Dev Cell.* 2005;9:535–543.
37. Knight PG, Glistner C. TGF- $\beta$  superfamily members and ovarian follicle development. *Reproduction.* 2006;132:191–206.
38. Glistner C, Kemp CF, Knight PG. Bone morphogenetic protein (BMP) ligands and receptors in bovine ovarian follicle cells: actions of BMP-4, -6 and -7 on granulosa cells and differential modulation of Smad-1 phosphorylation by follistatin. *Reproduction.* 2004;127:239–254.
39. De Crescenzo G, Hinck CS, Shu Z, et al. Three key residues underlie the differential affinity of the TGF $\beta$  isoforms for the TGF $\beta$  type II receptor. *J Mol Biol.* 2006;355:47–62.
40. Olsson M, Zhivotovsky B. Caspases and cancer. *Cell Death Differ.* 2011;18:1441–1449.
41. Boulares AH, Zoltoski AJ, Contreras FJ, Yakovlev AG, Yoshihara K, Smulson ME. Regulation of DNASE1L3 endonuclease activity by poly(ADP-ribosylation) during etoposide-induced apoptosis. Role of poly(ADP-ribose) polymerase-1 cleavage in endonuclease activation. *J Biol Chem.* 2002;277:372–378.
42. Pangas SA, Woodruff TK. Production and purification of recombinant human inhibin and activin. *J Endocrinol.* 2002;172:199–210.
43. Martens JW, de Winter JP, Timmerman MA, et al. Inhibin interferes with activin signaling at the level of the activin receptor complex in Chinese hamster ovary cells. *Endocrinology* 1997;138:2928–2936.
44. Lebrun JJ, Vale WW. Activin and inhibin have antagonistic effects on ligand-dependent heteromerization of the type I and type II activin receptors and human erythroid differentiation. *Mol Cell Biol.* 1997;17:1682–1691.
45. Iemura S, Yamamoto TS, Takagi C, et al. Direct binding of follistatin to a complex of bone-morphogenetic protein and its receptor inhibits ventral and epidermal cell fates in early *Xenopus* embryo. *Proc Natl Acad Sci USA.* 1998;95:9337–9342.
46. Wolfrum LA, Fernandez TM, Mamura M, et al. Loss of Smad3 in acute T-cell lymphoblastic leukemia. *N Engl J Med.* 2004;351:552–559.
47. Malickal TT, Antony ML, Nair A, Paulmurugan R, Karunakaran D. Loss of expression, and mutations of Smad 2 and Smad 4 in human cervical cancer. *Oncogene.* 2003;22:4889–4897.
48. Hahn SA, Schutte M, Hoque AT, et al. DPC4, a candidate tumor suppressor gene at human chromosome 18q21.1. *Science.* 1996;271:350–353.
49. Xu X, Brodie SG, Yang X, et al. Haploid loss of the tumor suppressor Smad4/Dpc4 initiates gastric polyposis and cancer in mice. *Oncogene.* 2000;19:1868–1874.
50. Schutte M. DPC4/SMAD4 gene alterations in human cancer, and their functional implications. *Ann Oncol.* 1999;10(suppl 4):56–59.
51. Takei K, Kohno T, Hamada K, et al. A novel tumor suppressor locus on chromosome 18q involved in the development of human lung cancer. *Cancer Res.* 1998;58:3700–3705.
52. Yu C, Zhang YL, Fan HY. Selective Smad4 knockout in ovarian preovulatory follicles results in multiple defects in ovulation. *Mol Endocrinol.* 2013;27:966–978.
53. Koinuma D, Tsutsumi S, Kamimura N, Imamura T, Aburatani H, Miyazono K. Promoter-wide analysis of Smad4 binding sites in human epithelial cells. *Cancer Sci.* 2009;100:2133–2142.
54. Kennedy BA, Deatherage DE, Gu F, et al. ChIP-seq defined genome-wide map of TGF $\beta$ /SMAD4 targets: implications with clinical outcome of ovarian cancer. *PLoS One.* 2011;6:e22606.
55. Wang W, Chen X, Li X, et al. Interference RNA-based silencing of endogenous SMAD4 in porcine granulosa cells resulted in decreased FSH-mediated granulosa cells proliferation and steroidogenesis. *Reproduction.* 2011;141:643–651.
56. Wang W, Wang L, Li XX, et al. Effect of interrupted endogenous BMP/Smad signaling on growth and steroidogenesis of porcine granulosa cells. *J Zhejiang Univ Sci B.* 2010;11:719–727.
57. Park SM, Jung JS, Jang MS, Kang KS, Kang SK. Transforming growth factor- $\beta$ 1 regulates the fate of cultured spinal cord-derived neural progenitor cells. *Cell Prolif.* 2008;41:248–264.
58. Teramoto T, Kiss A, Thorgeirsson SS. Induction of p53 and Bax during TGF- $\beta$ 1 initiated apoptosis in rat liver epithelial cells. *Biochem Biophys Res Commun.* 1998;251:56–60.
59. Xiao M, Oppenlander BK, Dooley DC. Transforming growth factor- $\beta$ 1 induces apoptosis in CD34<sup>+</sup>CD38<sup>low</sup> cells that express Bcl-2 at a low level. *Exp Hematol.* 2001;29:1098–1108.
60. Wicz Z, Sadkowski T, Jank M, Motyl T. Transcriptional pattern of TGF- $\beta$ 1 inhibitory effect on mouse C2C12 myoblasts differentiation. *Pol J Vet Sci.* 2010;13:629–638.
61. Yao G, Yin M, Lian J, et al. MicroRNA-224 is involved in transforming growth factor- $\beta$ -mediated mouse granulosa cell proliferation and granulosa cell function by targeting Smad4. *Mol Endocrinol.* 2010;24:540–551.
62. Zhang Y, Takahashi S, Tasaka A, Yoshima T, Ochi H, Chayama K. Involvement of microRNA-224 in cell proliferation, migration, invasion, and anti-apoptosis in hepatocellular carcinoma. *J Gastroenterol Hepatol.* 2013;28:565–575.